Excitation of phonons and forward focusing in x-ray photoemission from the valence band

M. A. Vicente Alvarez, H. Ascolani, and G. Zampieri
Centro Atómico Bariloche and Instituto Balseiro, Comisión Nacional de Energía Atómica, 8400-Bariloche, Argentina
(Received 17 July 1996)

A model is presented to explain the transition of the angular distribution of valence-band photoelectrons from the low-energy regime, characterized by emission only along the Mahan cones, to the high-energy regime, characterized by emission patterns very similar to those of core-level photoelectron diffraction. The two main ingredients of the model are the excitation/absorption of phonons during the photoemission, and the multiple scattering of the electron in the final state. Using simple assumptions about the valence-band initial states of Al(001) and a Debye model to describe the lattice vibrations, we calculate angular distributions of photoelectrons that are in excellent agreement with recent experimental results. [S0163-1829(96)06643-X]

I. INTRODUCTION

The energy- and angle-resolved photoemission of valence-band (VB) electrons has two regimes. At low energies there is a strict wave-vector conservation rule and the electrons are emitted along directions, known as Mahan directions,[1] defined by

$$\vec{k}_{f\parallel}=\vec{k}_{i\parallel}+\vec{g}_{hk},$$

where $\vec{k}_{i\parallel}$ and $\vec{k}_{f\parallel}$ are the wave vectors parallel to the surface in the initial and the final states of the electron, and $\vec{g}_{hk}$ is a vector of the surface reciprocal lattice. At high energies the excitation of phonons during the photoemission completely relaxes this wave-vector conservation rule, and the electrons are emitted in all directions. The transition from one regime to the other was studied first by Shevchik[2] and then by Fadley and co-workers.[3] They found that in a first approximation the photocurrent can be written as

$$I(\varepsilon)=e^{-2W}I_{\mathrm{DT}}(\varepsilon)+(1-e^{-2W})I_{\mathrm{NDT}}(\varepsilon),$$

where I_{DT} is the contribution of the $\vec{k}_{\parallel}$-conserving or ''direct'' transitions and I_{NDT} is the contribution of the non $\vec{k}_{\parallel}$-conserving or ''nondirect'' transitions; the exponent of the Debye-Waller factor is $W=\frac{1}{2}|\Delta\vec{k}^2|\langle u_z^2\rangle$, where $\Delta\vec{k}$ is the wave-vector change of the electron and $\langle u_z^2\rangle$ is the mean-square thermal displacement of the atoms.

In a recent letter, Osterwalder *et al.*[4] reported that in Al(001), at $h\nu=1254$ eV, the angular distribution of VB photoelectrons presents strong maxima of intensity at the main crystallographic directions and minor peaks at other directions, resembling very closely the angular distribution of photoelectrons from the $2s$ core level. This was quite unexpected because, unlike the core states, the VB states of Al are known to be completely delocalized, and because one expects that, at high energies, when all the peaks corresponding to the direct transitions have vanished, the angular distribution shall be rather smooth and only slightly structured.

The occurrence of maxima of intensity at the main internuclear directions is a well-known phenomenon in core-level x-ray photoemission.[5–7] In this case, the localized nature of the core state plays a crucial role; the wave representing the photoemitted electron emerges from a *single* atomic site and, on its way to the surface, interferes with the secondary waves produced by the scattering on the neighboring atoms. The maxima of intensity at the main internuclear directions are caused by a special type of interference called *forward focusing*.

To explain why at high photon energies the VB photoemission looks like the emission from a single atomic site, Osterwalder *et al.*[4] postulated a localization of the hole left behind by the photoelectron. Sarma *et al.*[8] criticized this argument, saying that if such localization occurred, the energy spectrum should exhibit some atomiclike character, which is not observed in the case of Al. They argued that the reason was the complete zone averaging caused by both the limited angular resolution and the energy integration performed by Osterwalder *et al.* Herman *et al.*[9] made the experiment in W(110) at 295 and 803 K, and argued that another cause could be the zone averaging produced by the excitation of phonons during the photoemission. However, to our knowledge, no one has presented a mathematical model to illustrate how these effects would produce the observed maxima of intensity at the main crystallographic directions.

This transition from a $\vec{k}_{\parallel}$-conserving regime at low energies to a non-$\vec{k}_{\parallel}$-conserving regime dominated by forward focusing at high energies is of the same kind as the one observed in the ''elastic'' backscattering of electrons from crystalline surfaces. In these experiments one observes a low-energy electron-diffraction (LEED)-like angular distribution of electrons at low energies that changes to an x-ray photoelectron diffraction (XPD)-like angular distribution at medium energies.[7,10,11] Since we have successfully modeled this last transition by including the excitation/absorption of phonons in a cluster-type LEED model,[12] it seemed natural to extend that work to the field of VB photoemission. Therefore, in this paper we present a model which explains the experimental results of Osterwalder *et al.* in terms of the excitation/absorption of phonons during the photoemission. Using simple assumptions about the VB initial states and a Debye model to describe the lattice vibrations, we calculate an angular distribution of photoelectrons that is in excellent agreement with the experimental results. Our approach is similar in many aspects to the one in the works of Shevchik.[2]

The key difference is our inclusion of multiple scattering in the final state. In this way we account for both the relaxation of the wave-vector conservation rule and the forward focusing at high energies.

The paper is organized as follows: in the Sec. II we present the model. In Sec. III we present the results of a calculation based on the model and compare with the experimental results of Osterwalder *et al.* In Sec. IV we analyze the role played by the phonons in the transition. Finally, in Sec. V we summarize our main results.

II. THEORY

A. Transition rate

We want to analyze the effect of including the vibrational degrees of freedom of the lattice in the photoemission of an electron from the valence band. Therefore, besides considering the interaction of the active electron with the radiation field, we must consider explicitly its interaction with the atoms of the vibrating semi-infinite crystal. This is done in the Appendix, where we show that the probability per unit time of emission of an electron with energy ε_f along the direction $\hat{k}_f$ from an initial (bound) state with energy ε_i and wave vector parallel to the surface $\vec{k}_{i\|}$ can be written as

$$\mathcal{R}=\frac{1}{\hbar^2}\int_{-\infty}^{\infty} dt\; e^{i(\varepsilon_f-\varepsilon_i-h\nu)t/\hbar}\langle\langle b_{if}(\{\vec{R}\})^* b_{if}(\{\vec{R}\},t)\rangle\rangle \tag{1}$$

where $h\nu$ is the photon energy,

$$b_{if}(\{\vec{R}\})=\langle \Psi^{LEED}_{-\vec{k}_f}(\{\vec{R}\})^*|-\frac{e}{mc}\vec{A}\cdot\vec{p}|\Phi_i(\{\vec{R}\})\rangle \tag{2}$$

is the photoemission matrix element calculated for the crystal with the atoms displaced from the equilibrium positions to positions indicated by $\{\vec{R}\}$, and

$$b_{if}(\{\vec{R}\},t)=e^{iH_{\rm ph}t/\hbar}b_{if}(\{\vec{R}\})e^{-iH_{\rm ph}t/\hbar} \tag{3}$$

is the photoemission matrix element in the interaction picture, with $H_{\rm ph}$ the Hamiltonian of the vibrating lattice, and where the symbol $\langle\langle\ \rangle\rangle$ denotes the thermal average of the argument over the phonon states of the lattice [see Eq. (A5)]. In Eq. (2) above, $\vec{A}$ is the vector potential of the radiation field, $\vec{p}$ is the momentum operator of the electron, and $|\Phi_i(\{\vec{R}\})\rangle$ and $|\Psi^{\rm LEED}_{-\vec{k}_f}(\{\vec{R}\})^*\rangle$ are eigenstates of the electron Hamiltonian with the lattice atoms at positions $\{\vec{R}\}$. $|\Phi_i(\{\vec{R}\})\rangle$ is the initial state of the electron, and $|\Psi^{\rm LEED}_{-\vec{k}_f}(\{\vec{R}\})^*\rangle$ is the time-reversed LEED state corresponding to an electron impinging on the crystal with energy ε_f along the direction $-\hat{k}_f$.[1,13]

Note that ε_f need not be equal to $\varepsilon_i+h\nu$. In particular, if $\varepsilon_f\neq\varepsilon_i+h\nu$ we calculate the transition rate of a photoemission event in which the photoelectron gives to or takes from the lattice an energy $\hbar\omega=\varepsilon_f-\varepsilon_i-h\nu$. If we neglect the lattice vibrations, the transition rate takes the usual form

$$\mathcal{R}=\frac{1}{\hbar^2}|b_{if}|^2\delta(\varepsilon_f-\varepsilon_i-h\nu).$$

To go further we need expressions in the coordinate space for the states $|\Phi_i(\{\vec{R}\})\rangle$ and $|\Psi^{\rm LEED}_{-\vec{k}_f}(\{\vec{R}\})^*\rangle$. We will use direct generalizations of known expressions for the case in which all the atoms are at rest at the equilibrium positions. These generalizations will be valid provided the displacements of the atoms from the equilibrium positions remain small.

Inside the solid,[14] the bound states of a semi-infinite crystal with wave vector $\vec{k}_{i\|}$ can be constructed as a combination of the states of the infinite crystal with the same energy and $\vec{k}_{i\|}$. If we choose ε_i near the bottom of the valence band, only two states will enter in the combination, one propagating toward the surface and the other reflected back at the surface. Therefore, in the tight-binding approximation, we have

$$\langle\vec{r}|\Phi_i(\{\vec{R}\})\rangle=\sum_n\ (e^{i\vec{k}_i^{+}\cdot\vec{R}_n}+\Re\ e^{i\vec{k}_i^{-}\cdot\vec{R}_n})\,\phi_i(\vec{r}-\vec{R}_n), \tag{4}$$

where $\vec{k}_i^{\pm}=\vec{k}_{i\|}\pm k_{iz}\hat{z}$, with k_{iz} a root of the equation $\varepsilon(\vec{k}_{i\|},k_{iz})=\varepsilon_i$, where $\varepsilon(\vec{k})$ is the dispersion relation of the infinite crystal. $\phi_i(\vec{r}-\vec{R}_n)$ is a combination of atomic orbitals centered at $\vec{R}_n$, and $\Re$ is the reflection coefficient. The sum in Eq. (4) runs over all the atoms of the semi-infinite crystal.

For the final state we will use a cluster-type expansion of the LEED wave function:[11,15]

$$\langle\vec{r}|\Psi^{\rm LEED}_{-\vec{k}_f}(\{\vec{R}\})^*\rangle=\Bigg[e^{i(-\vec{k}_f)\cdot\vec{r}}+\sum_n\ \psi_n(\vec{r})+\sum_n\sum_{n'\neq n}\psi_{nn'}(\vec{r})+\cdots\Bigg]^*, \tag{5}$$

where $-\vec{k}_f=-(2m\varepsilon_f/\hbar^2)^{1/2}\hat{k}_f$ is the wave vector of the incident electron, ψ_n is the wave originated in the scattering of the plane wave by the atom at $\vec{R}_n$, $\psi_{nn'}$ is the wave originated in the scattering of the wave ψ_n by the atom at $\vec{R}_{n'}$, and so on. The sums in Eq. (5) also run over all the atoms of the semi-infinite crystal.

The next step is to replace Eqs. (4) and (5) in Eq. (2). At this point we will make some simplifying assumptions: we will set $\Re$ equal to zero, $\vec{A}$ constant, and we will consider explicitly only the first two terms on the right side of Eq. (5). The derivation of the terms corresponding to $\Re\neq 0$ is straightforward, and we will incorporate them directly into our final results. Setting $\vec{A}$ constant is justified because the photon wave vector is in general so much smaller than the electron wave vectors that one can neglect it (dipolar approximation). At the end one can recover the main effect of the spatial variation of $\vec{A}$ replacing in the equations $\vec{k}_{i\|}$ by $\vec{k}_{i\|}+\vec{q}_{\rm photon\|}$. These two simplifications are only for the sake of mathematical simplicity. The purpose of the third approximation is to retain only the minimum basis set required to account for effects like the forward focusing. This is known in core-level photoemission as the ''single-scattering approximation.'' Inclusion of more terms in Eq. (5) is justified only if one needs better quantitative agreement with the ex-

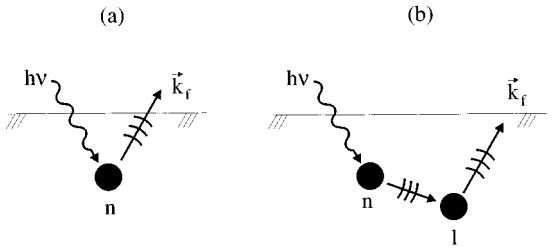

FIG. 1. Schematic representation of the electron paths corresponding to: (a) a direct wave (DW) and (b) a single-scattering wave (SSW).

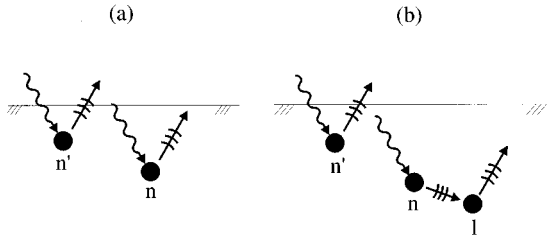

FIG. 2. Schematic representation of the interferences that contribute to the first and second terms of Eq. (10): (a) interference between two DW's and (b) interference between a DW and a SSW.

periment or to give account of effects like *defocusing*,[16] which are beyond the single-scattering approximation.[17] To obtain a simple expression for $b_{if}(\{\vec{R}\})$ we still need to make a further approximation. In replacing Eqs. (4) and (5) in Eq. (2) we will have to integrate $\psi_n(\vec{r})$ in the neighborhood of the atom at $\vec{R}_l$. To make this we will approximate the *spherical* wave $\psi_n(\vec{r})$ in the region around $\vec{R}_l$ by a *plane* wave with wave vector $\vec{k}_{ln}=k_f\,\hat{R}_{ln}$ $(\vec{R}_{ln}=\vec{R}_l-\vec{R}_n)$.[11]

Now the photoemission amplitude $b_{if}(\{\vec{R}\})$ can be set as

$$b_{if}(\{\vec{R}\})=\sum_n b_n^+ + \sum_n \sum_{l\neq n} b_{nl}^+, \tag{6}$$

where

$$b_n^+ = e^{i\Delta\vec{k}^+\cdot\vec{R}_n} M(\vec{k}_f) e^{-L_n/2\lambda} \tag{7}$$

and

$$b_{nl}^+ = e^{i\Delta\vec{k}_1^+\cdot\vec{R}_n} M(\vec{k}_{ln}) \frac{1}{R_{ln}} e^{i\Delta\vec{k}_2\cdot\vec{R}_l} f(\theta_{f,ln}) e^{-L_{nl}/2\lambda}, \tag{8}$$

with $\Delta\vec{k}^+=\vec{k}_i^+-\vec{k}_f$, $\Delta\vec{k}_1^+=\vec{k}_i^+-\vec{k}_{ln}$, $\Delta\vec{k}_2=\vec{k}_{ln}-\vec{k}_f$, $f(\theta)$ the elastic-scattering amplitude, $\theta_{f,ln}$ the angle between $\hat{k}_f$ and $\hat{k}_{ln}$, and

$$M(\vec{k})=\int d^3r\; e^{-i\vec{k}\cdot\vec{r}}\vec{A}_0\cdot\vec{p}\,\phi_i(\vec{r}). \tag{9}$$

Since $M(\vec{k})$ is the matrix element for the photoelectric transition from the initial state $\phi_i(\vec{r})$ to the final state $e^{i\vec{k}\cdot\vec{r}}$, we can view b_n^+ as the amplitude of the wave emitted from the atom at $\vec{R}_n$ directly into the direction $\hat{k}_f$, and b_{nl}^+ as the amplitude of the wave emitted from the atom at $\vec{R}_n$ in the direction $\hat{k}_{ln}$ and then redirected toward $\hat{k}_f$ by the (elastic) scattering at $\vec{R}_l$. Figures 1(a) and 1(b) show schematically the electron paths corresponding to the direct wave (DW) and the single-scattering wave (SSW), respectively. Note that $\Delta\vec{k}^+$ and $\Delta\vec{k}_1^+$ are the wave-vector changes in the photoelectric transitions, while $\Delta\vec{k}_2$ is the wave vector change in the scattering at $\vec{R}_l$.

In the second term on the right-hand side of Eq. (6), we omitted the terms b_{nn}^+ because they are not amplitudes of SSW's but first-order corrections to the amplitudes b_n^+ by considering the change of the (plane-wave) final state caused by the potential of the emitting atom. In Eqs. (7) and (8) we also introduced the effect of the inelastic collisions of the photoemitted electron with the other electrons of the crystal by weighting each amplitude with an attenuation factor $e^{-L/2\lambda}$, where L is the total electron path inside the solid (from the photoemission site to the surface) and λ is the electron mean free path. Finally, in the derivation of Eqs. (7) and (8) we made use of the translational symmetry parallel to the surface to exchange the order in the evaluation of the sum over atoms with the spatial integration. This is a valid procedure only when the displacements of the atoms from the equilibrium positions remain small.

Having written $b_{if}(\{\vec{R}\})$ in terms of the amplitudes b_n^+ and b_{nl}^+, we can obtain a similar expression for $b_{if}(\{\vec{R}\},t)$. Then, it only remains to make the thermal average of the product $b_{if}(\{\vec{R}\})^* b_{if}(\{\vec{R}\},t)$, for which we make two last approximations: (i) we keep the dependences of b_n^+ and b_{nl}^+ on the displacements of the atoms from the equilibrium positions, $\vec{u}_n=\vec{R}_n-\vec{R}_n^{\,0}$, only in the phase factors; and (ii) we assume that the lattice vibrations can be treated within the harmonic approximation. Then, we can use the Glauber formula[18] $\langle\langle e^{iA}\rangle\rangle = e^{-1/2\langle\langle A^2\rangle\rangle}$ and obtain

$$\begin{aligned}\mathcal{R}=\frac{1}{\hbar^2}\int_{-\infty}^{\infty} dt\; e^{i\omega t}\Bigg\{ &\sum_{n,n'} (b_{n'}^+)^* b_n^+ e^{-W_{n'}(\Delta\vec{k}^+)} \\ &\times e^{-W_n(\Delta\vec{k}^+)} e^{\langle\langle[\Delta\vec{k}^+\cdot\vec{u}_{n'}][\Delta\vec{k}^+\cdot\vec{u}_n(t)]\rangle\rangle} \\ &+ 2\,\mathrm{Re}\sum_{n,n'}\sum_{l\neq n} (b_{n'}^+)^* b_{nl}^+\, e^{-W_{n'}(\Delta\vec{k}^+)} e^{-W_n(\Delta\vec{k}_1^+)} \\ &\times e^{-W_l(\Delta\vec{k}_2)} e^{-\langle\langle[\Delta\vec{k}_1^+\cdot\vec{u}_n][\Delta\vec{k}_2\cdot\vec{u}_l]\rangle\rangle} \\ &\times e^{\langle\langle[\Delta\vec{k}^+\cdot\vec{u}_{n'}][\Delta\vec{k}_1^+\cdot\vec{u}_n(t)]\rangle\rangle + \langle\langle[\Delta\vec{k}^+\cdot\vec{u}_{n'}][\Delta\vec{k}_2\cdot\vec{u}_l(t)]\rangle\rangle}\Bigg\},\end{aligned} \tag{10}$$

where b_n^+ and b_{nl}^+ are now evaluated for the crystal with the atoms at the equilibrium positions $\{\vec{R}^{\,0}\}$, $\hbar\omega=\varepsilon_f-\varepsilon_i-h\nu$, and $W_n(\vec{k})=\frac{1}{2}\langle\langle[\vec{k}\cdot\vec{u}_n(t)]^2\rangle\rangle$. The first term in this equation is the sum of the interferences of two DW's emitted at different times, and the second term is the sum of the interferences of a DW and a SSW emitted at different times. Both types of interferences are shown schematically in Fig. 2. We omitted for simplicity the term corresponding to the interferences of two SSW's emitted at different times.

Equation (10) is our final expression for the transition rate $\mathcal{R}$. It gives the transition rate from the initial state $(\varepsilon_i,\vec{k}_{i\|})$ to the state $(\varepsilon_f,\hat{k}_f)$ in terms of the inelastic energy $\hbar\omega$, the photoemission amplitudes b_n^+ and b_{nl}^+ (calculated for the crystal with the atoms fixed at the equilibrium positions), and the time-dependent correlation functions $\langle\langle[\vec{k}_A\cdot\vec{u}_n][\vec{k}_B\cdot\vec{u}_l(t)]\rangle\rangle$. The first term of this equation is the result derived previously by Shevchik;[2] the only difference would be in the election of the final state for the matrix element $M(\vec{k})$, which is a plane wave in our case and an augmented plane wave in Shevchik's treatment. The second term of the equation contains the multiple-scattering effects. This term, which is absent in Shevchik's treatment, is the one which will give rise to the XPD-like angular patterns at high photoelectron energies.

B. Phonon expansion

The phonon expansion of $\mathcal{R}$ consists of replacing in Eq. (10) the exponentials of the time-dependent correlation functions by their Taylor series[26,12]

$$e^{\langle\langle[\vec{k}_A\cdot\vec{u}_n][\vec{k}_B\cdot\vec{u}_l(t)]\rangle\rangle}=\sum_{m=0}^{\infty}\frac{\langle\langle[\vec{k}_A\cdot\vec{u}_n][\vec{k}_B\cdot\vec{u}_l(t)]\rangle\rangle^m}{m!}. \quad (11)$$

In this way one can speak of the $m=0$, 1, etc. contributions to $\mathcal{R}$. In the $m=0$ contribution to $\mathcal{R}$ the two time-dependent exponentials in Eq. (10) are replaced by one. Then, the quantity within braces in Eq. (10) loses its time dependence, and the integration of $e^{i\omega t}$ gives a $\delta(\omega)$ factor. Therefore, the $m=0$ contribution to $\mathcal{R}$ is different from zero only when $\varepsilon_f=\varepsilon_i+h\nu$, i.e., it is the elastic or zero-phonon contribution. One can further show that this contribution is different from zero only when $\vec{k}_{f\|}=\vec{k}_{i\|}+\vec{g}_{hk}$. Then, in the elastic photoemission events the electrons emerge from the crystal only along a discrete set of directions, which are precisely the Mahan directions.

In the $m=1$ contribution to $\mathcal{R}$ the two time-dependent exponentials in Eq. (10) are replaced by their arguments. In this case, since the time dependence of the displacements $\vec{u}_l(t)$ is through phase factors of the form $e^{\pm i\omega_\alpha(\vec{Q}_\|)t}$, where $\omega_\alpha(\vec{Q}_\|)$ is the frequency of the phonon mode of wave vector $\vec{Q}_\|$ and quantum number α, the time integral gives terms proportional to $\delta(\omega\pm\omega_\alpha(\vec{Q}_\|))$. Then, the $m=1$ contribution to $\mathcal{R}$ is composed of many terms (two terms per phonon mode), and is different from zero only when $\varepsilon_f=\varepsilon_i+h\nu\mp\hbar\omega_\alpha(\vec{Q}_\|)$, i.e., it represents the contribution to $\mathcal{R}$ of the photoemission events with excitation or absorption of one phonon. It can also be shown that this contribution is different from zero only when $\vec{k}_{f\|}=\vec{k}_{i\|}+\vec{g}_{hk}\mp\vec{Q}_\|$. Therefore, in the photoemission events in which one phonon is excited or absorbed, the electrons also emerge from the crystal only along a discrete set of directions.

In general, if several phonons are excited and/or absorbed during a photoemission event, the electron will emerge from the crystal only along a discrete set of directions with $\vec{k}_{f\|}=\vec{k}_{i\|}+\vec{g}_{hk}-\Sigma_\mu\sigma_\mu\vec{Q}_\|^{(\mu)}$ where $\sigma_\mu=1$ if a phonon of wave vector $\vec{Q}_\|^{(\mu)}$ is excited and $\sigma_\mu=-1$ if it is absorbed. This conservation law is a direct consequence of the translational symmetry of the problem.

Therefore, both elastic and inelastic photoemission events obey strict wave-vector conservation rules that restrict severely the exit directions of the photoelectron. However, we will show below that the sum of the intensities of many inelastic photoemission events gives rise to an intensity pattern which is very similar to the core-level intensity patterns.

C. Observed intensity

Let us consider an ideal energy- and angle-resolved photoemission experiment with an infinite energy resolution $(\Delta\varepsilon=0)$. Then, the intensity of the electrons photoemitted in the direction $\hat{k}_f$ with energy ε_f will be proportional to $\mathcal{R}(\varepsilon_i,\vec{k}_{i\|};\varepsilon_f,\hat{k}_f)$ summed over all the occupied initial states $(\varepsilon_i,\vec{k}_{i\|})$. In real experiments $\Delta\varepsilon$ is not zero but of the order of 1 eV. Then, the *observed* intensity will be

$$I_{\rm obs}(\varepsilon_f,\hat{k}_f)\propto\int_{\varepsilon_f-\Delta\varepsilon}^{\varepsilon_f+\Delta\varepsilon}\sum_i^{\rm occupied}\mathcal{R}(\varepsilon_i,\vec{k}_{i\|};\varepsilon_f',\hat{k}_f)d\varepsilon_f'.$$

Exchanging the order of the integral and the sum, and integrating over $\hbar\omega=\varepsilon_f'-\varepsilon_i-h\nu$ instead of over ε_f', the *observed* intensity can be set as

$$I_{\rm obs}(\varepsilon_f,\hat{k}_f)\propto\sum_i^{\rm occupied}\int_{-\infty}^{\infty}\mathcal{R}(\varepsilon_i,\vec{k}_{i\|};\hbar\omega,\hat{k}_f)d(\hbar\omega),$$

where we assumed that, since $\Delta\varepsilon$ is much larger than the phonon energies, the limits of the integral can be extended from $(-\Delta\varepsilon,+\Delta\varepsilon)$ to $(-\infty,+\infty)$. Now, if we neglect the dependence of k_f on $\hbar\omega$,[19] the only dependence of $\mathcal{R}(\varepsilon_i,\vec{k}_{i\|};\hbar\omega,\hat{k}_f)$ on $\hbar\omega$ is through the phase factor $e^{i\omega t}$; then the integration over ω gives a $\delta(t)$ function, and the integration over t gives the quantity within braces in Eq. (10) evaluated at time $t=0$. Therefore, recovering the terms corresponding to $\Re\neq0$, the final expression for the *observed* intensity is

$$\begin{aligned}I_{\rm obs}(\varepsilon_f,\hat{k}_f)\propto\sum_i^{\rm occupied}\sum_{\sigma,\sigma'}\Bigg\{&\sum_{n,n'}(b_{n'}^{\sigma})^*b_n^{\sigma'}e^{-W_{n'}(\Delta\vec{k}^{\sigma})}\\&\times e^{-W_n(\Delta\vec{k}^{\sigma'})}e^{\langle\langle[\Delta\vec{k}^{\sigma}\cdot\vec{u}_{n'}][\Delta\vec{k}^{\sigma'}\cdot\vec{u}_n]\rangle\rangle}\\&+2\,{\rm Re}\sum_{n,n'}\sum_{l\neq n}(b_{n'}^{\sigma})^*b_{nl}^{\sigma'}e^{-W_{n'}(\Delta\vec{k}^{\sigma})}e^{-W_n(\Delta\vec{k}_1^{\sigma'})}\\&\times e^{-W_l(\Delta\vec{k}_2)}e^{-\langle\langle[\Delta\vec{k}_1^{\sigma'}\cdot\vec{u}_n][\Delta\vec{k}_2\cdot\vec{u}_l]\rangle\rangle}\\&\times e^{\langle\langle[\Delta\vec{k}^{\sigma}\cdot\vec{u}_{n'}]\Delta[\vec{k}_1^{\sigma'}\cdot\vec{u}_n]\rangle\rangle+\langle\langle[\Delta\vec{k}^{\sigma}\cdot\vec{u}_{n'}][\Delta\vec{k}_2\cdot\vec{u}_l]\rangle\rangle}\Bigg\},\end{aligned} \quad (12)$$

where the index σ takes the values + and −, and where b_n^- and b_{nl}^- are the equivalents of b_n^+ and b_{nl}^+ [i.e., Eqs. (7) and (8) with $\vec{k}_i^+$ replaced by $\vec{k}_i^-$] multiplied by the reflection coefficient $\Re$.

It is easy to see in Eq. (12) that, at low energies, when all the exponentials approach 1, one has essentially the interfer-

ence of waves emitted from a two-dimensional array of atoms, and thus intensity only in the Mahan directions. As the energy is increased the exponentials cannot be ignored anymore, and one starts to have intensity outside the Mahan directions. This transition will be analyzed in the next sections.

Finally, to evaluate Eq. (12) we need to define the correlation functions $\langle\langle[\vec{k}_A\cdot\vec{u}_n][\vec{k}_B\cdot\vec{u}_l(t)]\rangle\rangle$, which requires the formulation of a model for the lattice vibrations. We will use the Debye model $\omega=cq$, for which the correlation functions can be written as[20]

$$\langle\langle[\vec{k}_A\cdot\vec{u}_n][\vec{k}_B\cdot\vec{u}_l(t)]\rangle\rangle=(\vec{k}_A\cdot\vec{k}_B)\sigma^2(\theta)F(q_DR_{nl},\theta), \tag{13}$$

where $\theta=T/\theta_D$, $\sigma^2(\theta)$ is the mean-square amplitude of vibration of the atoms,

$$\sigma^2(\theta)=\frac{3\hbar^2}{4Mk_B\theta_D}\left[1+4\theta^2\int_0^{1/\theta}\frac{z\,dz}{e^z-1}\right],$$

and the function $F(x,\theta)$ is almost independent of θ, and falls rapidly from one to zero when x increases[21] (θ_D and q_D are the Debye temperature and wave vector, respectively).

III. RESULTS

In this section we present angular distributions of electrons photoemitted from Al(001) calculated with Eq. (12). The calculations were performed for three selected initial states, so we have not summed over all the occupied initial states as indicated in Eq. (12). This simplification allows us to identify the main structures in the angular distributions in an easy way and, as we will see, it is not an impediment to compare with the experimental results. We have used the three initial states shown in Fig. 3. The states, labeled A, B, and C, have energy $\varepsilon_i=-7.2$ eV and wave vectors along the $\bar{\Sigma}$ line $\vec{k}_{i\|}=2\pi/a(\alpha,0,0)$ with $\alpha=0$, $\frac{1}{3}$, and $\frac{2}{3}$. The components k_{iz}^{+} associated with each state were determined from the dispersion relation $\varepsilon(\vec{k})$ of Al calculated by Moruzzi, Janak, and Williams (MJW).[23] The reflection coefficient $\Re$ was calculated assuming a constant potential inside the solid and a step potential at the surface of 15.4 eV, which corresponds to the energy difference between the vacuum level of Al(001) and the Γ point in the band structure of MJW. $f(\theta)$ was computed by the standard partial-wave method for the muffin-tin potential of MJW. The refraction of the photoelectron at the surface was included by considering an inner potential of 8.4 eV, which is the energy difference between the vacuum level and the muffin-tin zero. The photoelectric matrix element $M(\vec{k})$ was taken to be spherically symmetric. We used inelastic mean free paths calculated according to Ref. 24 and a Debye temperature $\theta_D=254$ K (lower than the bulk value to allow for the larger displacements of the atoms at the surface). The correlation function $F(x,\theta)$ was considered only for pairs of atoms separated by a distance smaller than or equal to a lattice constant; for the other cases $F(x,\theta)$ was set equal to zero. The sums over scatterers in the SSW's were extended to all the atoms within a distance of 2.5 lattice constants of the emitter. Finally, to simulate the experimental angular resolution, we integrated the intensities over a cone of $\pm3°$.

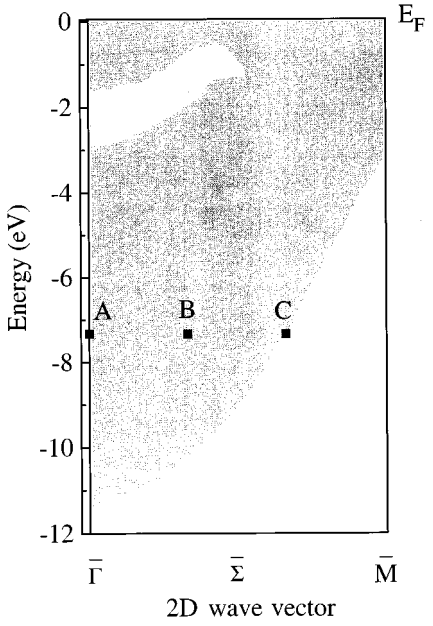

FIG. 3. Projected band structure of Al(001) along the $\bar{\Sigma}$ line (adapted from Ref. 22). A, B, and C indicate the three initial states used in the calculations. The energies are given with respect to the Fermi level.

Figure 4 shows polar intensity plots (PIP's) along the [100] azimuth calculated for the three initial states and at three different photoelectron energies. The arrows in the PIP's at 105 and 550 eV indicate the polar angles at which the Mahan directions of the state labeled A enter into the

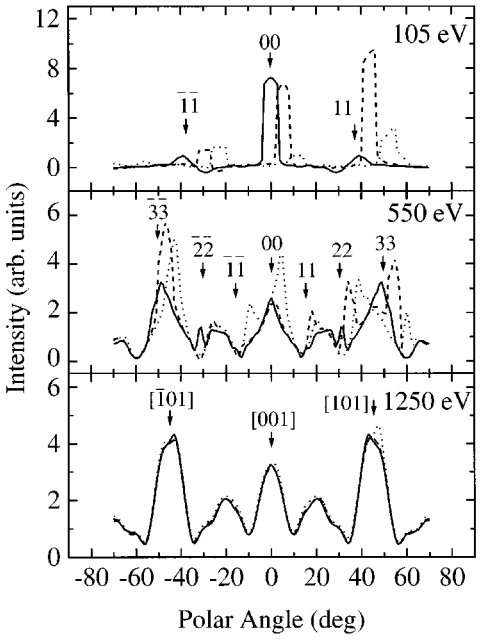

FIG. 4. Polar intensity plots along the [100] azimuth calculated for the three initial states of Fig. 3. The solid line corresponds to the state labeled A, the broken line to the state labeled B, and the dotted line to the state labeled C. The meaning of the arrows is explained in the text.

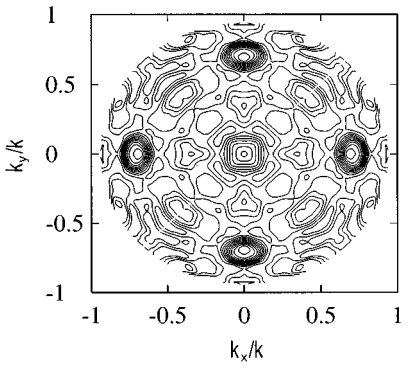

FIG. 5. Contour plot of the photoemission intensity corresponding to the state labeled A at a photoelectron energy of 1250 eV ($k = 18.1$ Å^{-1}).

analyzer, whereas in the PIP at 1250 eV they indicate the polar angles at which the main crystallographic directions enter into the analyzer. The PIP's corresponding to the state labeled A are symmetric with respect to $\theta=0$ due to the symmetry of this state with respect to reflections in the plane yz. It is seen that at 105 eV all the intensity is concentrated in the Mahan directions. This means that at this energy the photoemission is dominated by the direct transitions. There are three Mahan directions for each initial state that enter into the analyzer in this angular scan; for the state labeled A this occurs at $\theta=0$ and $\sim\pm40°$. The peaks corresponding to the states labeled B and C are shifted with respect to those of the state A because of the finite wave vectors $\vec{k}_{i\|}$. At 550 eV there are more direct transitions allowed but on the average they are less intense than at 105 eV. There is more intensity outside the Mahan directions and, in particular, the three states give rise to important intensity in the regions around 0, $\pm20°$, and $\pm45°$. At 1250 eV the PIP's corresponding to the three initial states are almost converged on a common PIP which is very similar to the PIP's observed in core-level XPD. There are broad peaks at 0 and $\pm45°$, corresponding to emission along the crystallographic axes $[\bar{1}01]$, [001], and [101], and smaller structures at $\sim\pm20°$. Neither the positions of these peaks nor the general form of the PIP's change when one increases more the photoelectron energy. Therefore, the angle-resolved VB photoemission is state selective only at low photoelectron energies. At high photoelectron energies the emission from any initial state has a PIP similar to those observed in core-level XPD, irrespective of the state and to a good extent of the photoelectron energy.

Figure 5 presents a contour plot of the photoemission intensity corresponding to the state labeled A at a photoelectron energy of 1250 eV. There are five major peaks that coincide with the crystallographic directions [001], [011], $[0\bar{1}1]$, [101], and $[\bar{1}01]$. All these peaks are caused by the forward-focusing effect (zero-order interference between a DW and a SSW originated in the same atom). Outside these directions the intensity falls 4–5 times; there are some minor peaks near the directions [103], [013], $[\bar{1}03]$, $[0\bar{1}3]$ and [112], $[\bar{1}12]$, $[\overline{1\,1\,2}]$, $[1\bar{1}2]$, which are caused by first-order interferences between a DW and SSW originated in the same atom. The contour plots, corresponding to states labeled B and C, are very similar to the one shown in Fig. 5, with only minor differences concentrated mainly in the regions of the five major peaks.

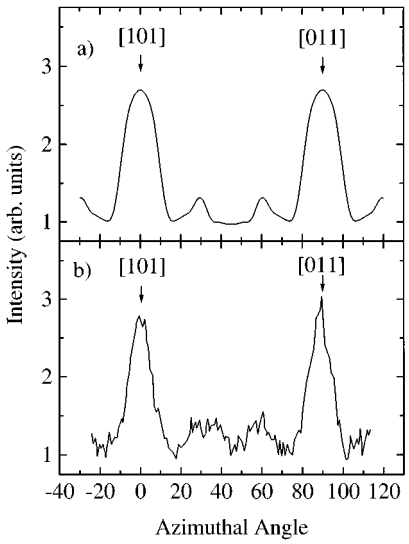

FIG. 6. Azimuthal intensity plots at $\theta = 45°$: (a) AIP calculated for the state labeled A at a photoelectron energy of 1250 eV; (b) experimental AIP (from Ref. 4).

In their photoemission experiment, Osterwalder *et al.*[4] measured the azimuthal intensity plot (AIP) at $\theta=45°$ of all the electrons photoemitted from the VB. An angular scan of this type is a circumference in the contour plot of Fig. 5. In Fig. 6 we compare the calculated intensity for the state labeled A with the intensity measured by Osterwalder *et al.* It is seen that the calculated AIP reproduces all the features of the experimental AIP. There are two peaks at $\phi=0$ and 90° (corresponding to emission along the crystallographic directions [101] and [011]) and two smaller structures at $\phi\sim30°$ and 60°. The main discrepancies between the calculated and experimental AIP's are that in the calculated AIP the main peaks are broader than in the experimental AIP while the structures at 30° and 60° are narrower. We ascribe these small differences to our use of a single-scattering approximation; the inclusion of higher-order scattering terms should improve the agreement.

IV. DISCUSSION

In the previous section we have seen that our model for the VB photoemission reproduces correctly the two types of angular distributions observed at low and high energies. In this section we will analyze the interplay of the elastic and inelastic contributions to the intensity. To this purpose we will use the phonon expansion of Sec. II B. Repeating the procedure made to obtain Eq. (12) with the $m=0$ and $m=1$ contributions to $\mathcal{R}$, one obtains the contributions to the *observed* intensity of the zero- and one-phonon photoemission events. It turns out that this procedure is equivalent to make a phonon expansion of Eq. (12), i.e., to replace in this equation the exponentials of $\langle\langle[\Delta\vec{k}^{\sigma}\cdot\vec{u}_{n'}][\Delta\vec{k}^{\sigma'}\cdot\vec{u}_{n}]\rangle\rangle$ and of $\langle\langle[\Delta\vec{k}^{\sigma}\cdot\vec{u}_{n'}][\Delta\vec{k}_1^{\sigma'}\cdot\vec{u}_{n}]\rangle\rangle+\langle\langle[\Delta\vec{k}^{\sigma}\cdot\vec{u}_{n'}][\Delta\vec{k}_2\cdot\vec{u}_{n}]\rangle\rangle$ by their Taylor series.[12] Then, the elastic or zero-phonon contribution to $I_{\rm obs}$ is

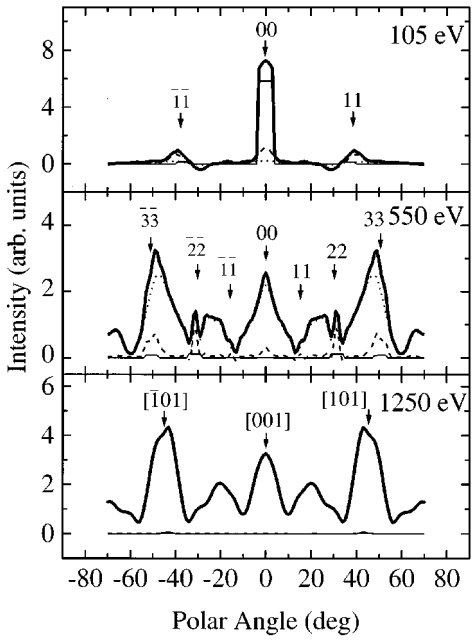

FIG. 7. Decomposition of the PIP's of Fig. 4 corresponding to the state labeled *A* into the three phonon contributions defined in the text: zero phonon (thin solid line), one phonon (broken line), and multiphonon (dotted line).

$$I^{(0)}_{\rm obs}(\varepsilon_f,\hat{k}_f)\propto \sum_{i}^{\rm occupied}\sum_{\sigma,\sigma'}\left\{\sum_{n,n'}(b^{\sigma}_{n'})^{*}b^{\sigma'}_{n}\right.$$
$$\times e^{-W_{n'}(\Delta\vec{k}^{\sigma})}e^{-W_{n}(\Delta\vec{k}^{\sigma'})}$$
$$+2\,{\rm Re}\sum_{n,n'}\sum_{l\neq n}(b^{\sigma}_{n'})^{*}b^{\sigma'}_{nl} \qquad (14)$$
$$\times e^{-W_{n'}(\Delta\vec{k}^{\sigma})}e^{-W_{n}(\Delta\vec{k}_1^{\sigma'})}e^{-W_{l}(\Delta\vec{k}_2)}$$
$$\left.\times e^{-\langle\langle[\Delta\vec{k}_1^{\sigma'}\cdot\vec{u}_n][\Delta\vec{k}_2\cdot\vec{u}_l]\rangle\rangle}\right\} \qquad (15)$$

and the contribution to $I_{\rm obs}$ of *all* the one-phonon photoemission events is

$$I^{(1)}_{\rm obs}(\varepsilon_f,\hat{k}_f)\propto \sum_{i}^{\rm occupied}\sum_{\sigma,\sigma'}\left\{\sum_{n,n'}(b^{\sigma}_{n'})^{*}b^{\sigma'}_{n}e^{-W_{n'}(\Delta\vec{k}^{\sigma})}\right.$$
$$\times e^{-W_{n}(\Delta\vec{k}^{\sigma'})}\langle\langle[\Delta\vec{k}^{\sigma}\cdot\vec{u}_{n'}][\Delta\vec{k}^{\sigma'}\cdot\vec{u}_n]\rangle\rangle$$
$$+2\,{\rm Re}\sum_{n,n'}\sum_{l\neq n}(b^{\sigma}_{n'})^{*}b^{\sigma'}_{nl}e^{-W_{n'}(\Delta\vec{k}^{\sigma})}$$
$$\times e^{-W_{n}(\Delta\vec{k}_1^{\sigma'})}e^{-W_{l}(\Delta\vec{k}_2)}e^{-\langle\langle[\Delta\vec{k}_1^{\sigma'}\cdot\vec{u}_n][\Delta\vec{k}_2\cdot\vec{u}_l]\rangle\rangle}$$
$$\times(\langle\langle[\Delta\vec{k}^{\sigma}\cdot\vec{u}_{n'}][\Delta\vec{k}_1^{\sigma'}\cdot\vec{u}_n]\rangle\rangle$$
$$\left.+\langle\langle[\Delta\vec{k}^{\sigma}\cdot\vec{u}_{n'}][\Delta\vec{k}_2\cdot\vec{u}_l]\rangle\rangle)\right\}. \qquad (16)$$

Finally, we define a multiphonon contribution to $I_{\rm obs}$ as the difference between Eq. (12) and Eqs. (14) and (15).

Figure 7 shows the decomposition of the PIP's of Fig. 4 corresponding to the state labeled *A* into the three contributions defined above. The thin solid line in the figures corresponds to the elastic or zero-phonon contribution, the broken line to the one-phonon contribution, and the dotted line to the multiphonon contribution. It is seen in the PIP's at 105 and 550 eV that, as explained in Sec. II B, the zero-phonon component is different from zero only at the Mahan directions. The width of the peaks of this contribution is determined solely by the angular acceptance of the analyzer, whereas their intensities are determined by the interference of waves emitted from atoms in different layers and by the Debye-Waller factors. It is also seen in these two PIP's that the one-phonon contribution is also different from zero only around the Mahan directions. In this case the width of the peaks is determined by both the angular resolution and by the average wave vector of the phonon involved in the transition. Therefore, the narrowness of the peaks of this contribution is indicating that the excitation or absorption of phonons with $Q\approx 0$ is the dominant process.

The PIP at 105 eV is dominated by the zero- and one-phonon components. The main contribution to the central peak comes from the zero-phonon component, while the main contributions to the two minor peaks come from the one-phonon component. The multiphonon contribution is almost negligible over the entire PIP. At 550 eV the multiphonon component has had an enormous increase and makes the main contribution to the total intensity; the one-phonon component is the second most important contribution, while the zero-phonon component has become negligibly small. The multiphonon component gives rise to structures at 0, $\pm 20°$, and $\pm 45°$, whereas the one-phonon component is responsible for the peaks at the (2 2) and (22) Mahan directions (only direct transitions seen clearly in the PIP) and partly for the peaks at $\pm 49°$. Finally, at 1250 eV, when the PIP has reached its (core-level) XPD-like final form, the zero- and one-phonon components are completely negligible and the PIP is due entirely to the multiphonon component.

Therefore, we can conclude that the $\vec{k}_{\parallel}$-conserving regime at low photoelectron energies and the XPD-like regime at high energies correspond to the limiting cases of completely elastic photoemission and of inelastic photoemission with excitation/absorption of multiple phonons.

The transition from the elastic to the inelastic regime is governed by the Debye-Waller factors as explained in Refs. 2 and 3. The differences between the two types of photoemission that cause the different angular patterns are the following. In elastic photoemission, due to the wave-vector conservation rule, the electrons are emitted only along the Mahan directions. The forward focusing cannot show up in this regime because the Mahan directions rarely coincide with the internuclear axes. In the inelastic photoemission, particularly when several phonons are excited and/or absorbed, the restrictions imposed by the wavevector conservation rules are counterbalanced by the continuous supply of phonon wave vector; this relaxes the electronic wave-vector conservation rule and allows the forward focusing to produce intensity enhancements at the main internuclear directions. Therefore, the evolution of the angular distribution of photoelectrons as the energy is increased is explained as follows. At sufficiently low energies the probability of the inelastic

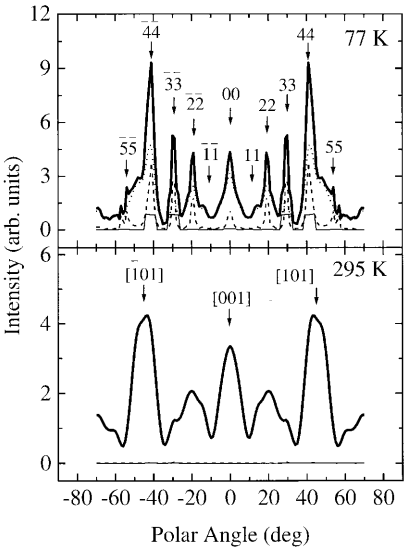

FIG. 8. PIP's along the [100] azimuth calculated for the state labeled *A* at a photoelectron energy of 1250 eV and at two temperatures: 77 and 295 K. Both PIP's are decomposed into the three phonon contributions; the correspondence of the lines with the contributions is as in Fig. 7.

events is negligible; the photoemission is dominated by the elastic events, and the electrons are emitted only along the Mahan directions. Increasing the energy decreases the probability of the elastic photoemission and increases the probability of the inelastic events. The first inelastic events to turn on are the one-phonon photoemission events; however, since the average wave vector of the phonon involved in the transition is small, the emission is still concentrated in the Mahan directions. Increasing the energy further increases the probability of the inelastic events that involve larger numbers of phonons and larger total wave vectors exchanged with the lattice. Eventually, at a certain energy all the emission directions become more or less equally probable, except those near the main internuclear axes which benefit from the forward focusing. In this way, the relaxation of the electronic wave vector conservation rule combined with the forward focusing produce the enhanced intensities at the main internuclear directions.

We will finish this section with two considerations regarding the other causes postulated to explain the transition from the $\vec{k}_{\parallel}$-conserving regime to the XPD-like regime. First, we note that two of the proposed causes (the hole localization and the phonon excitation) are intrinsic to the photoemission process, while the other obeys external parameters (the angular and energy resolutions). With respect to this latter, we have shown above that at room temperature, at high photon energies the excitation/absorption of multiple phonons will always lead to XPD-like angular patterns, irrespective of the angular and energy resolutions. In other words, we have shown that at room temperature and high photon energies it is impossible to set back to the $\vec{k}_{\parallel}$-conserving regime by improving the angular and/or energy resolutions alone. This could only be achieved if one in addition cools down the crystal to suppress the excitation/absorption of phonons. This is shown in Fig. 8, where we compare the PIP's calculated for the state labeled *A* at room temperature and at liquid N_2 temperature. It is seen in the figure that lowering the crystal temperature down to the liquid N_2 temperature one recovers practically all the peaks corresponding to the $\vec{k}_{\parallel}$-conserving regime.[25] One could now use this change of the PIP with the temperature to test the validity of the hole localization argument. The test would be based on the assumption that this effect, if present, should depend mainly on the photon energy and should be approximately independent of the crystal temperature. Therefore, cooling the crystal to suppress the excitation/absorption of phonons, in the absence of hole localization, at high photoelectron energies the angular pattern should transform as discussed above, showing again direct transitions (with enough angular and energy resolutions), but, if hole localization does occur, the angular pattern should retain its XPD-like character, approximately independent of the temperature and of the angular and energy resolutions.

V. CONCLUSIONS

The purpose of this work has been to analyze the nature of the transition in VB photoemission from the low-energy or $\vec{k}_{\parallel}$-conserving regime to the high-energy or XPD-like regime.

Three possible causes have been put forward to explain this transition: localization of the hole at high photoelectron energies,[4] complete zone averaging due to poor angular resolution and energy integration,[8] and excitation and/or absorption of phonons during the photoemission.[9] In this paper we have demonstrated that the transition can be explained completely in terms of the excitation and/or absorption of phonons. Therefore, this transition is of the same kind as the one occurring in the elastic scattering of electrons from crystalline surfaces, where there is a $\vec{k}_{\parallel}$-conserving or LEED-like regime at low energies, and a non-$\vec{k}_{\parallel}$-conserving or XPD-like regime at high energies.

We have presented a treatment of the VB photoemission that takes into account both the vibrational degrees of freedom of the lattice and the multiple scattering of the electron in the final state. The first is needed to explain the relaxation of the electron wave-vector conservation rule, and the second is needed to explain the maxima of intensity at the main crystallographic directions that are observed in the high-energy regime. Using a phonon expansion of the transition rate, we have shown that the low-energy or $\vec{k}_{\parallel}$-conserving regime and the high-energy or XPD-like regime correspond to the limiting cases of completely elastic scattering and of inelastic scattering with excitation/absorption of multiple phonons, respectively. We performed a calculation based on this model that is in very good agreement with the experimental results of Osterwalder *et al.*[4]

ACKNOWLEDGMENTS

We acknowledge partial support by the CONICET. One of us (M.A.V.A.) wants to acknowledge I. Samengo for fruitful discussions.

APPENDIX

In this appendix we will derive an expression for the probability per unit time of emission of an electron with

energy ε_f along the direction $\hat{k}_f$ from an initial state with energy ε_i and wave vector parallel to the surface $\vec{k}_{i\parallel}$ considering the vibrational degrees of freedom of the crystal lattice.

The Hamiltonian of the electron interacting with the radiation field and with the atoms of the vibrating lattice is

$$H=H_{\rm ph}+H_{\rm el}+\Delta U(\vec{r},\{\vec{R}\})+H_{\rm rad}+U_{\rm rad}, \tag{A1}$$

where $H_{\rm ph}$ is the Hamiltonian that describes the lattice vibrations, $H_{\rm el}=\vec{p}^{\,2}/2m+U(\vec{r},\{\vec{R}^{\,0}\})$ is the Hamiltonian of the electron moving in the semi-infinite crystal with the atoms fixed at the equilibrium positions, $\Delta U(\vec{r},\{\vec{R}\})=U(\vec{r},\{\vec{R}\})-U(\vec{r},\{\vec{R}^{\,0}\})$ is the part of the potential that couples the electronic and the atomic motions ($\vec{r}$ and $\{\vec{R}\}$ denote the electron and the atomic positions, respectively), $H_{\rm rad}$ is the Hamiltonian of the radiation field, and $U_{\rm rad}$ is the interaction potential between the electron and the radiation field.

The basis set used to analyze this problem is composed of the eigenstates of the Hamiltonians $H_{\rm ph}$, $H_{\rm el}$, and $H_{\rm rad}$. Mahan[1] and Feibelman and Eastman[13] have shown that the eigenstates of $H_{\rm el}$ relevant to the photoemission problem are the initial state $|\Phi_i(\{\vec{R}^{\,0}\})\rangle$, with energy ε_i and wave vector parallel to the surface $\vec{k}_{i\parallel}$, and the final state $|\Psi^{\rm LEED}_{-\vec{k}_f}(\{\vec{R}^{\,0}\})^*\rangle$, the time-reversed LEED state corresponding to an electron impinging on the crystal with energy ε_f along the direction $-\hat{k}_f$. Then, the transition probability per unit time is

$$\begin{aligned}\mathcal{R}=\frac{2\pi}{\hbar}\sum_{|f\rangle}\sum_{|i\rangle}&|\langle\Psi^{\rm LEED}_{-\vec{k}_f}(\{\vec{R}^{\,0}\})^*|\langle f|\langle n|\tau(\varepsilon_i+\Omega_i\\&+(n+1)h\nu)|n+1\rangle|i\rangle|\Phi_i(\{\vec{R}^{\,0}\})\rangle|^2\frac{e^{-\Omega_i/k_BT}}{Z}\\&\times\delta(\Omega_f-\Omega_i+\varepsilon_f-\varepsilon_i-h\nu),\end{aligned} \tag{A2}$$

where $|n+1\rangle$ and $|n\rangle$ are the states of the radiation field with $n+1$ and n photons of frequency ν, respectively, and $|i\rangle$ and $|f\rangle$ are the initial and final vibrational states of the lattice with energies Ω_i and Ω_f, respectively. We have summed over all the final states of the lattice and over all the initial states populated at temperature T (Z is the partition function of the vibrating lattice). The transition operator $\tau(E)$ can be written in terms of the Green operator G of the unperturbed Hamiltonian $H_{\rm ph}+H_{\rm el}+H_{\rm rad}$ as

$$\tau(E)=\Delta U+U_{\rm rad}+(\Delta U+U_{\rm rad})G(E)(\Delta U+U_{\rm rad})+\cdots. \tag{A3}$$

Using the integral representation of the δ function one can eliminate in Eq. (A2) the sum over the final states of the lattice;[26] then,

$$\begin{aligned}\mathcal{R}=\frac{1}{\hbar^2}\int_{-\infty}^{\infty}dt\;e^{i(\varepsilon_f-\varepsilon_i-h\nu)t/\hbar}\langle\langle\;&\langle\Psi^{\rm LEED}_{-\vec{k}_f}(\{\vec{R}^{\,0}\})^*|\\&\times\langle n|\tau(\varepsilon_i+\Omega_i+(n+1)h\nu)|n+1\rangle|\Phi_i(\{\vec{R}^{\,0}\})\rangle^*\\&\times\langle\Psi^{\rm LEED}_{-\vec{k}_f}(\{\vec{R}^{\,0}\})^*|\langle n|\tau(\varepsilon_i+\Omega_i+(n+1)h\nu;t)|n+1\rangle\\&\times\Phi|_i(\{\vec{R}^{\,0}\})\rangle\;\rangle\rangle,\end{aligned} \tag{A4}$$

where $\tau(E;t)$ is the time-dependent transition operator in the interaction picture,

$$\tau(E;t)=e^{iH_{\rm ph}t/\hbar}\tau(E)e^{-iH_{\rm ph}t/\hbar},$$

and where the symbol $\langle\langle\;\rangle\rangle$ denotes the thermal average of the argument over the initial states of the lattice populated at temperature T:

$$\langle\langle{\rm O}(\{\vec{R}\})\rangle\rangle=\sum_{|i\rangle}\langle i|O(\{\vec{R}\})|i\rangle\frac{e^{-\Omega_i/k_BT}}{Z}. \tag{A5}$$

We will now make two approximations: (i) In Eq. (A3) we will keep only the terms linear in $U_{\rm rad}$. Then, the transition operator becomes

$$\tau(E)=\Delta U+[\cdots+\Delta UG(E)+1]U_{\rm rad}[1+G(E)\Delta U+\cdots]$$

and the matrix elements of τ between the states of the radiation field result:

$$\begin{aligned}&\langle n|\tau(\varepsilon_i+\Omega_i+(n+1)h\nu)|n+1\rangle\\&\quad=[\cdots+\Delta UG_0(\varepsilon_i+\Omega_i+h\nu)+1]\\&\qquad-\frac{e}{mc}\vec{A}\cdot\vec{p}[1+G_0(\varepsilon_i+\Omega_i)\Delta U+\cdots],\end{aligned}$$

where we have used

$$\langle n|U_{\rm rad}|n+1\rangle=-\frac{e}{mc}\vec{A}\cdot\vec{p},$$

where $\vec{A}$ is the vector potential of the radiation field in the Coulomb gauge and $\vec{p}$ is the momentum operator of the electron. $G_0(E)$ is the Green operator of the unperturbed Hamiltonian $H_{\rm ph}+H_{\rm el}$, which is written in terms of the eigenstates of $H_{\rm el}$ ($|\Phi_n\rangle$ with energy ε_n) and $H_{\rm ph}$ ($|\lambda\rangle$ with energy Ω_λ) as

$$G_0(E)=\sum_{|\Phi_n\rangle}\sum_{|\lambda\rangle}\frac{|\Phi_n\rangle|\lambda\rangle\langle\lambda|\langle\Phi_n|}{E-\varepsilon_n-\Omega_\lambda}. \tag{A6}$$

(ii) *Adiabatic* approximation. In Eq. (A6) we will neglect the phonon energies, which are 10^4–10^5 times smaller than the electron energies. Then, $G_0(\varepsilon+\Omega)$ becomes $g_0(\varepsilon)$, the Green operator of the electron moving in the semi-infinite crystal with the atoms fixed at the equilibrium positions, and the matrix element of $\langle n|\tau(E)|n+1\rangle$ between the states $|\Phi_i(\{\vec{R}^{\,0}\})\rangle$ and $|\Psi^{\rm LEED}_{-\vec{k}_f}(\{\vec{R}^{\,0}\})^*\rangle$ can be set as (using $\varepsilon_f=\varepsilon_i+h\nu$)

$$\langle \Psi^{\mathrm{LEED}}_{-\vec{k}_f}(\{\vec{R}^{\,0}\})^* | \langle n | \tau(\varepsilon_i+\Omega_i+(n+1)h\nu) | n+1\rangle | \Phi_i(\{\vec{R}^{\,0}\})\rangle$$

$$= \langle \Psi^{\mathrm{LEED}}_{-\vec{k}_f}(\{\vec{R}\})^* | -\frac{e}{mc}\vec{A}\cdot\vec{p} | \Phi_i(\{\vec{R}\})\rangle, \qquad \text{(A7)}$$

where

$$|\Psi^{\mathrm{LEED}}_{-\vec{k}_f}(\{\vec{R}\})^*\rangle = [1+g_0(\varepsilon_f)\Delta U+\cdots]|\Psi^{\mathrm{LEED}}_{-\vec{k}_f}(\{\vec{R}^{\,0}\})^*\rangle$$

and

$$|\Phi_i(\{\vec{R}\})\rangle = [1+g_0(\varepsilon_i)\Delta U+\cdots]|\Phi_i(\{\vec{R}^{\,0}\})\rangle$$

are eigenstates of $H_{\mathrm{el}}+\Delta U(\vec{r},\{\vec{R}\})$, the Hamiltonian of the electron moving in the crystal with the atoms at arbitrary positions $\{\vec{R}\}$.

Now, replacing Eq. (A7) in Eq. (A4), the transition probability per unit time can be written as

$$\mathcal{R} = \frac{1}{\hbar^2}\int_{-\infty}^{\infty} dt\; e^{i(\varepsilon_f-\varepsilon_i-h\nu)t/\hbar}\langle\langle b_{if}(\{\vec{R}\})^* b_{if}(\{\vec{R}\},t)\rangle\rangle, \qquad \text{(A8)}$$

where

$$b_{if}(\{\vec{R}\}) = \left\langle \Psi^{\mathrm{LEED}}_{-\vec{k}_f}(\{\vec{R}\})^* \left| -\frac{e}{mc}\vec{A}\cdot\vec{p} \right| \Phi_i(\{\vec{R}\}) \right\rangle \qquad \text{(A9)}$$

is the photoemission matrix element calculated for the crystal with the atoms occupying positions denoted by $\{\vec{R}\}$, and

$$b_{if}(\{\vec{R}\},t) = e^{iH_{\mathrm{ph}}t/\hbar} b_{if}(\{\vec{R}\}) e^{-iH_{\mathrm{ph}}t/\hbar} \qquad \text{(A10)}$$

is the photoemission matrix element in the interaction picture.

[1] G. D. Mahan, Phys. Rev. B **2**, 4334 (1970).

[2] N. J. Shevchik, Phys. Rev. B **16**, 3428 (1977); **20**, 3020 (1971).

[3] R. C. White, C. S. Fadley, M. Sagurton, and Z. Hussain, Phys. Rev. B **34**, 5226 (1986); Z. Hussain, S. Kono, L. G. Peterson, C. S. Fadley, and L. F. Wagner, *ibid.* **23**, 724 (1981).

[4] J. Osterwalder, T. Greber, S. Hüfner, and L. Schlapbach, Phys. Rev. Lett. **64**, 2683 (1990).

[5] C. S. Fadley, in *Synchrotron Radiation Research: Advances in Surface Science*, edited by R. Z. Bachrach (Plenum, New York, 1990).

[6] W. F. Egelhoff, Crit. Rev. Solid State Mater. Sci. **16**, 213 (1990), and in *Ultrathin Magnetic Structures I, An Introduction to Electronic, Magnetic, and Structural Properties*, edited by J. A. C. Bland and B. Heinrich (Springer-Verlag, Berlin, 1994), Chap. 5.

[7] S. A. Chambers, Adv. Phys. **40**, 357 (1991); Surf. Sci. Rep. **16**, 261 (1992).

[8] D. D. Sarma, W. Speier, and J. F. van Acker, Phys. Rev. Lett. **66**, 2834 (1991).

[9] G. S. Herman, T. T. Tran, K. Higashiyama, and C. S. Fadley, Phys. Rev. Lett **68**, 1204 (1992).

[10] H. Ascolani, M. M. Guraya, and G. Zampieri, Phys. Rev. B **43**, 5135 (1991).

[11] H. Ascolani, R. O. Barrachina, M. M. Guraya, and G. Zampieri, Phys. Rev. B **46**, 4899 (1992).

[12] M. A. Vicente Alvarez, H. Ascolani, and G. Zampieri, Phys. Rev. B **53**, 7524 (1996).

[13] P. J. Feibelman and D. E. Eastman, Phys. Rev. B **10**, 4932 (1974).

[14] We neglect the contribution to Eq. (2) of the part of the initial-state wave function that decays exponentially in the vacuum.

[15] J. J. Barton, M.-L. Xu, and M. A. Van Hove, Phys. Rev. B **37**, 10 475 (1988).

[16] W. F. Egelhoff, Phys. Rev. Lett. **59**, 559 (1987).

[17] M.-L. Xu and M. A. Van Hove, Surf. Sci. **207**, 215 (1989); M.-L. Xu, J. J. Barton, and M. A. Van Hove, Phys. Rev. B **39**, 8275 (1989).

[18] N. D. Mermin, J. Math. Phys. **7**, 1038 (1966).

[19] Note that in terms of $\hbar\omega$ one has $\vec{k}_f = [2m(\varepsilon_i+h\nu+\hbar\omega)/\hbar^2]^{1/2}\hat{k}_f$.

[20] G. Beni and P. M. Platzman, Phys. Rev. B **14**, 1514 (1976).

[21] See Fig. 4 in Ref. 12.

[22] M. Heinrichsmeier, A. Fleszar, and A. M. Eguiluz, Surf. Sci. **285**, 129 (1993).

[23] V. L. Moruzzi, J. F. Janak, and A. R. Williams, *Calculated Electronic Properties of Metals* (Pergamon, New York, 1978).

[24] S. Tanuma, C. J. Powell, and D. R. Penn, Surf. Interf. Anal. **20**, 77 (1993).

[25] Note, however, that the PIP of Fig. 8(a) corresponds to the emission from only one initial state. In a real experiment, the emissions from several other initial states will also reach the detector unless one uses very high angular and energy resolutions.

[26] N. W. Ashcroft and N. D. Mermin, *Solid State Physics* (Saunders College, Philadelphia, 1976), Appendix N.